



# Evolution of defects and their effect on photoluminescence and conducting properties of green-synthesized ZnS nanoparticles

B. Lalitha Devi<sup>1</sup> · K. Mohan Rao<sup>1</sup> · Dhananjaya Kekuda<sup>1</sup> · D. Ramananda<sup>2</sup>

Received: 2 January 2018 / Accepted: 17 October 2018 / Published online: 24 October 2018  
© Springer-Verlag GmbH Germany, part of Springer Nature 2018

## Abstract

We have grown ZnS (zinc sulfide) nanoparticles (NPs) by hydrothermal and microwave (MW) heating method and a comparative study on the physical properties was carried out. Zinc acetate dihydrate (ZAD) and thioacetamide (TA) were used as Zn and S precursors, respectively. X-ray diffraction (XRD) and selected area electron diffraction (SAED) pattern revealed the cubic structure for ZnS and nanocrystalline nature of the samples. The careful observation of the XRD patterns of the samples grown by hydrothermal and microwave heating method indicate that microwave-synthesized ZnS (ZnS–MW) samples were strained compared to those grown by conventional hydrothermal methods. Uniform sized smaller nanoparticles were formed during microwave irradiation in a much shorter time. UV–Vis absorption spectra indicated quantum confinement effect. The emission peaks in photoluminescence spectra indicate the presence of various point defects in the samples. In the microwave synthesized sample, nucleation and growth process of the ZnS crystallites are very quick, leading to the formation of defects. The dielectric studies of both types of the samples show a typical behavior of polycrystalline semiconducting material. Under the applied A.C. fields, the conduction phenomena provide sufficient evidence for the electronic hopping between localized sites. Lower values of activation energy obtained for both dipolar relaxation and DC conductivity in the case of microwave synthesized sample indicate the applicability of such materials in various switching applications.

## 1 Introduction

In recent years, II–VI semiconductor nanomaterials such as ZnS, CdS, CdTe, ZnSe etc. have been the subject of intensive research interest owing to their size-dependent property of quantum confinement effect [1, 2]. Among them, ZnS is an important II–VI semiconducting material widely used as a phosphor which exhibits high luminous intensity and narrow emission band. Apart from the size-dependent

luminescence, emission in ZnS can also be tuned by incorporation of suitable impurities. Visible emission has been achieved in ZnS by inducing mid gap energy levels in the nano crystals of ZnS due to doping with metallic ions such as Ag, Ni, Mn etc. [2]. ZnS has been proved to be an efficient visible light driven photocatalyst for H<sub>2</sub> evolution. Some photocatalytic ZnS materials have also been investigated for the antimicrobial activities [3]. In addition, the nano-sized ZnS finds application in flat panel displays, solar cells, infrared windows, photoconductors, sensors etc [4–6]. Due to less toxicity, ZnS is also finding applications in biological labeling and diagnostics [7]. A lower value of activation energy for dielectric relaxation and electrical conduction is under investigation for the possible application of these defected materials in flash memory devices.

Majority of reports available in literature on the synthesis of ZnS nanomaterials include hydrothermal process [8], sol–gel method [9], chemical co-precipitation method [10], sonochemical method [11], microwave irradiation [12] and solvothermal method [13] etc. The size of the ZnS nanocrystallite was found to depend on the preparation conditions such as the ratio of metal salt to sulfur source, operating

✉ K. Mohan Rao  
mohan\_raok@yahoo.com

B. Lalitha Devi  
lalithadevibck@gmail.com

Dhananjaya Kekuda  
dhaya.kekuda@manipal.edu

D. Ramananda  
ramanandabak@gmail.com

<sup>1</sup> Department of Physics, Manipal Institute of Technology, Manipal Academy of Higher Education, Manipal, Karnataka 576104, India

<sup>2</sup> Department of Physics, Bhandarkars' Arts and Science College, Kundapura, Karnataka 576201, India

temperature and pressure during reaction, the amount of capping agents used, and method of heating the precursors.

In a conventional heating, an external thermal source heats the reaction medium by a conductive heating. This is an inefficient method of transferring energy into a system, as it depends on the thermal conductivity of different materials that must be penetrated [14]. This results in excess temperature of the reaction vessel which is much higher than that required for the reaction. In contrast, microwave irradiation produces efficient in-core volumetric heating by direct coupling of microwave energy with the molecules (solvents, reagents, catalysts) that are present in the reaction mixture. N Dahal et al. [15] have reported an extensive comparative study of conventional heating against microwave heating in noble metal nanoparticle (NP) synthesis and observed preferential effects of MW heating on nucleation and growth of near monodisperse Rh, Pd and Pt NPs. Zhu et al. have studied effect of microwave power on the size of ZnS nanoparticles (NPs). In their investigation, marginal size reduction of particles from 3 to 2.9 nm with decrease in microwave power from 650 to 280 W was reported [16, 17]. Ma et al. have reported the growth of ZnS NPs through conventional heating at 140 °C for 8 h, and have reported particles of 6.4 nm size [18]. Even though separate studies are available on the growth of ZnS NPs by conventional hydrothermal and microwave synthesis, comparative study of the ZnS NPs grown by these two techniques is not reported as per our best of knowledge. Hence such a comparative study has been carried out in the present work. The ability of a specific substance to convert electromagnetic energy of microwave into heat at a given frequency is determined by the dielectric loss factor  $\tan\delta$ . Water having  $\tan\delta = 0.123$ , classified as medium polar solvent, is best suited in our case for the synthesis of ZnS NPs to follow principles of green chemistry. The most common microwave frequency used for research is 2.45 GHz ( $\lambda \sim 12.25$  cm), the same as for the domestic microwave ovens. Since conventional heating and microwave heating processes are fundamentally different in their heating mechanisms, it will result in a vastly different product with different properties.

The objective of the present work is to synthesize ZnS nanoparticles (NPs) in aqueous dispersion by conventional and MW heating, and, to explore the method specific desired properties of ZnS NPs for device applications. The aqueous synthesis of ZnS is based on the heat sensitivity of thioacetamide (TA), which releases sulfur (S) species on heating. Consequently, the reaction was well activated under microwave irradiation resulting in the formation of ZnS nanocrystals in a much shorter time.

## 2 Experimental details

### 2.1 Synthesis by hydrothermal method

Zinc acetate dihydrate [ $\text{Zn}(\text{CH}_3\text{COO})_2 \cdot 2\text{H}_2\text{O}$ ] of molecular weight 219.5 and thioacetamide ( $\text{CH}_3\text{CSNH}_2$ ) of molecular weight 75.13 were used as zinc and sulphur precursors, respectively. The chemicals used were of AR grade and used without further purification. Initially, individual solutions of 0.15 M zinc acetate dihydrate and 0.27 M TA were prepared separately. They were mixed in a round bottomed flask (RBF) under stirring for 15 min at room temperature. This mixture was subsequently heated for 2 h at a constant temperature of 80 °C, with water cooled condenser fixed to the flask. The solution was then allowed to cool naturally to room temperature. ZnS NPs were separated by centrifugation, washed several times with double distilled water and finally washed with acetone. The precipitate was dried in a hot air oven and the resulted sample was named as ZnS–HT.

### 2.2 Synthesis by microwave heating method

For the microwave-assisted synthesis of sample, RBF containing a mixture of precursors was placed in a custom designed domestic microwave oven. It is worth mentioning that we have utilized the same starting materials and their concentration mentioned in the previous method for the microwave synthesis of ZnS. A water-cooled condenser was connected outside the microwave oven cavity by a glass joint to RBF. With reflux systems, there is little risk of explosions as the flammable vapors will not be released into the microwave cavity and the heating system will be at atmosphere pressure. Heating of precursors was done by microwave radiations for 6 min. Colloidal precipitate obtained was cooled to ambient temperature, washed, separated by centrifugation, dried and the resulted sample was named as ZnS–MW.

Synthesized samples were subjected to X-ray diffraction using Rigaku Miniflex 600 X-Ray Diffractometer operating at 40 kV and 15 mA with monochromatic copper— $K_\alpha$  radiation. Transmission electron microscope (TEM) studies were carried out using JOEL JEM 2100 High-Resolution Transmission Electron Microscope operating at 200 kV. Optical absorption spectrum was recorded using SHIMADZU-1800 UV–Vis spectrophotometer at room temperature. A Photoluminescence (PL) spectrum was obtained with the help of Hitachi F-7000 Fluorescence Spectrophotometer. Dielectric measurements were carried out using a Novocontrol Alpha Impedance Analyzer (Novocontrol Technologies, Germany) equipped with a quatro liquid nitrogen gas cryosystem, over a frequency range of 100 Hz–5 MHz at several temperatures between 223 K and 323 K.

### 3 Results and discussion

#### 3.1 X-ray diffraction

XRD pattern of samples synthesized by both the methods (conventional and MW heating) is shown in Fig. 1. The prominent broad peaks indicate nanocrystalline nature of the samples. The XRD peaks were corresponding to (111), (220) and (311) planes of simple cubic structure of ZnS as identified with JCPDS file nos.03-065-9585 and 01-071-5971 for the samples ZnS-HT and ZnS-MW respectively. Additional diffraction peaks due to impurities or other crystalline phases were not detected from the XRD pattern indicating the high purity of the grown nanoparticles.

Average crystallite size ( $D$ ) was calculated for the prominent (111) diffraction peak using Debye Scherrer equation:

$$D = \frac{0.9 \lambda}{\beta \cos \theta} \quad (1)$$

where  $\lambda$  is wavelength of incident X-rays;  $\theta$  is angle of diffraction,  $\beta$  is full width at half maximum (FWHM) of Bragg peak. Interplanar separation ( $d_{hkl}$ ) between planes corresponding to Miller indices ( $hkl$ ) were calculated using Bragg's law.

Strain ( $\varepsilon$ ) produced in the nanocrystallites was calculated using

$$\varepsilon = \frac{\beta}{4 \tan \theta} \quad (2)$$

Narrow X-ray diffraction peaks with increased intensity were observed for ZnS-HT samples compared to that of ZnS-MW samples, indicative of increased crystallinity [19] and particle size for ZnS-HT samples. Lee et al. [20] found a small increase in peak intensity with a slight decrease in line width with increase in synthesis temperature of ZnS:Cu nanocrystals, and it was attributed to the possibility of grain growth with temperature. The increased crystallinity and particle size for ZnS-HT samples in the present study may be due to prolonged synthesis procedure for ZnS-HT samples leading to crystal growth followed by agglomeration.

**Fig. 1** X-ray diffraction pattern for ZnS-HT and ZnS-MW samples

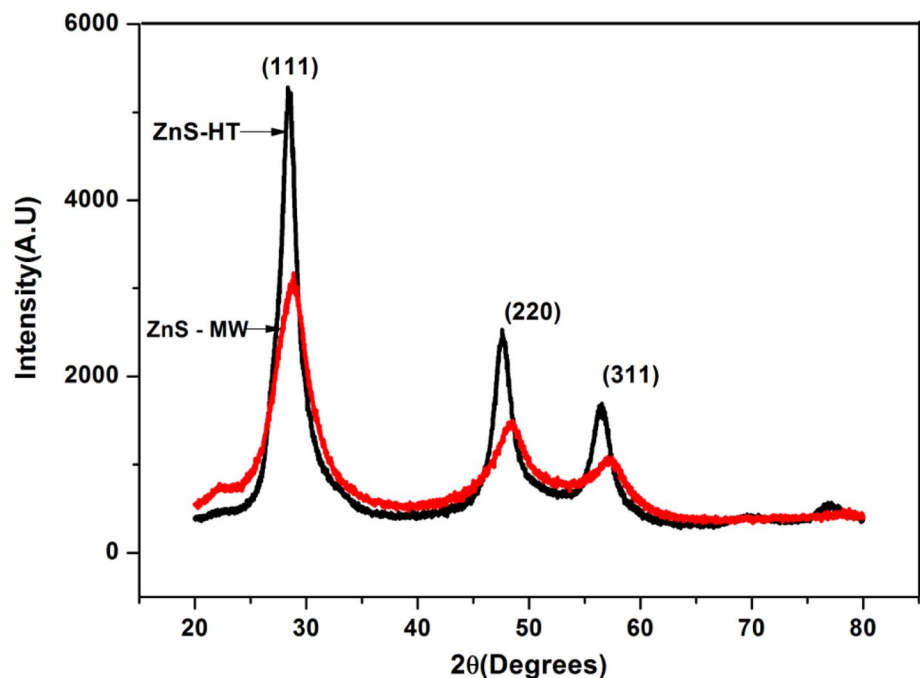


**Table 1** Percentage of elements present in ZnS-HT and ZnS-MW and their particle size

Sample	Atomic % of Zn	Atomic % of S	Strain, $\times 10^{-3}$	Crystallite size from XRD (nm)	NP size from TEM (nm)	NP size from UV-Vis absorption (nm)
ZnS-HT	51.8	48.2	36.13	3.89	6.3	6.1
ZnS-MW	55.5	45.5	65.22	2.13	2.55	2.9

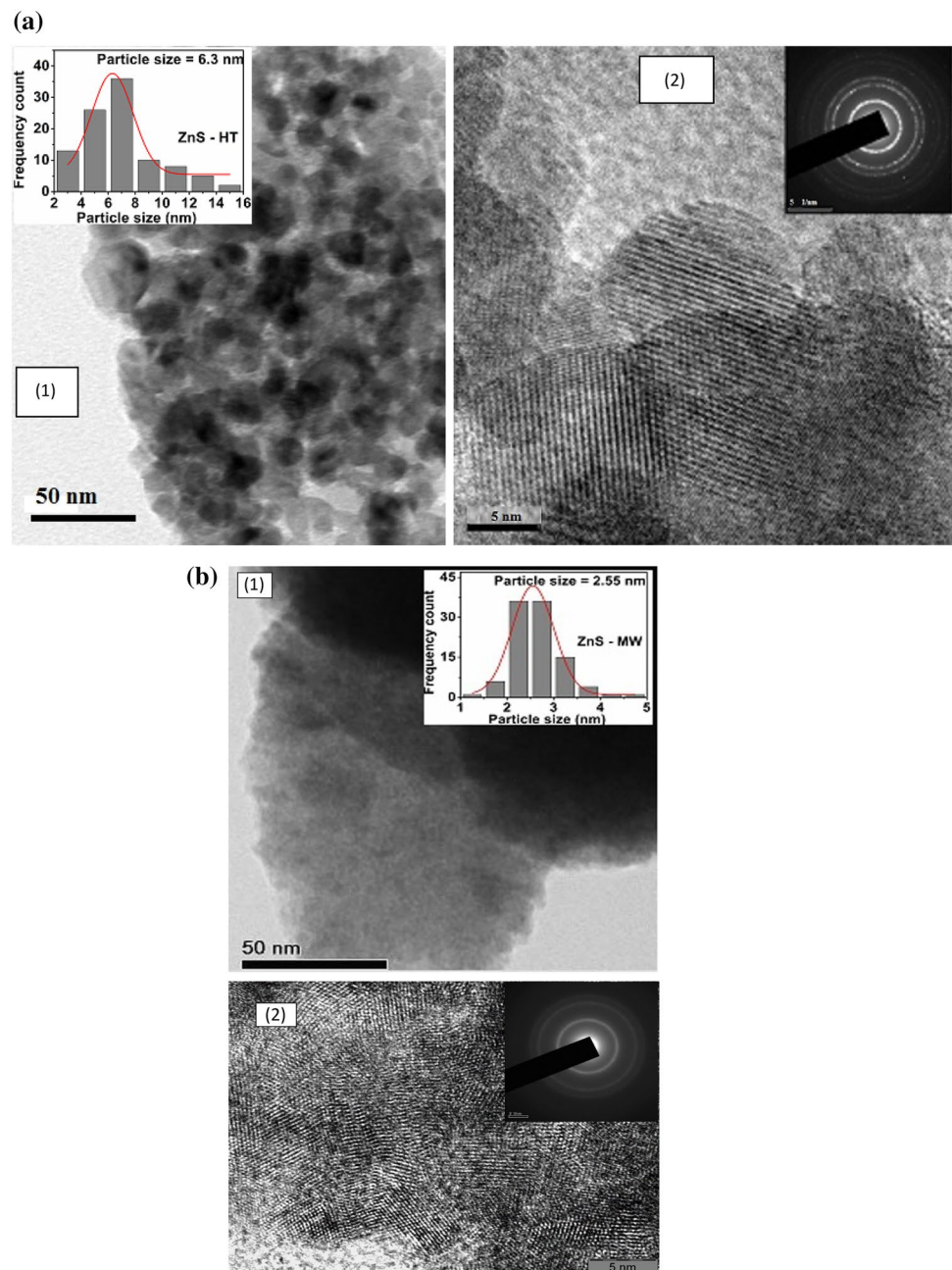
Lattice strain produced in the ZnS nanocrystallites synthesized by both the methods are given in Table 1. It is observed from the table that a higher lattice strain is developed for ZnS nanocrystallites synthesized by MW heating as compared to conventional heating. The inter-planar spacing  $d_{111}$  obtained for ZnS-HT is 3.123 Å, and it gets reduced to 3.111 Å for ZnS-MW.

### 3.2 Electron microscopy

Transmission electron microscopy (TEM) is less likely to be affected by experimental errors and more direct than X-ray

line broadening [21]. Figure 2a show the TEM, high-resolution TEM (HRTEM) image and selected area electron diffraction (SAED) pattern for ZnS-HT sample while Fig. 2b correspond to that of ZnS-MW sample. A close observation of the HRTEM figures reveal that smaller crystallites are resulted for the samples synthesized by MW heating as compared to the conventional heating. Size distribution of NPs are plotted for the TEM images of both samples and shown as insets in 2a(1) for ZnS-HT and 2b(1) for ZnS-MW. TEM images indicate the non formation of monosized NPs in the case of ZnS-HT sample. From the SAED pattern of both type of samples, it is inferred that the diffracting planes are

**Fig. 2** a (1) TEM and inset is histogram of distribution of particles and (2) HRTEM image for ZnS-HT sample and inset is SAED pattern. b (1) TEM and (2) HRTEM image for ZnS-MW and inset is SAED pattern



corresponding to (111), (220) and (311) planes of sphalerite ZnS. The presence of sharp spots in the SAED pattern of ZnS-HT is a measure of high crystallinity of the samples as observed from the XRD results. On the contrary, only diffraction rings were observed in the case of ZnS-MW indicating fine grain structure of the sample. Both the samples show agglomeration effect. But MW synthesized sample shows agglomeration tendency to a greater extent which may be due to the smallness of NPs, indicating the necessity of using a capping agent to get stabilized NPs.

EDS analysis of ZnS-HT and ZnS-MW showed the presence of Zn and S atoms in the prepared samples. As observed from the XRD spectra, EDS spectra did not show any traces of other elements which confirm the purity of the samples. The percentage of elements Zn and S obtained from EDS as well as crystallite sizes obtained by XRD, TEM and UV-Vis absorption studies are shown in Table 1.

### 3.3 Optical properties

#### 3.3.1 UV-absorption studies

The dependence of absorbance of samples on wavelength is shown in Fig. 3. The absorption peaks occur at 329 nm and 322 nm for ZnS-HT and ZnS-MW respectively. The marginal shift in the absorption peak towards lower wavelength observed for the ZnS-MW samples is attributed to particle size effect. For the samples prepared by both the methods, there is a blue shift of absorption peaks compared to that of

bulk (337 nm) which indicates strong quantum confinement effect. Band gap of ZnS NPs is calculated from the Tauc relation [22]:

$$\alpha h\nu = A(E_{h\nu} - E_g)^n \tag{3}$$

where  $\alpha$  is absorption coefficient, obtained by Beer Lamberts' principle and  $A$  is a constant;

$$\alpha = \frac{2.303 \text{ Absorbance}}{t} \tag{4}$$

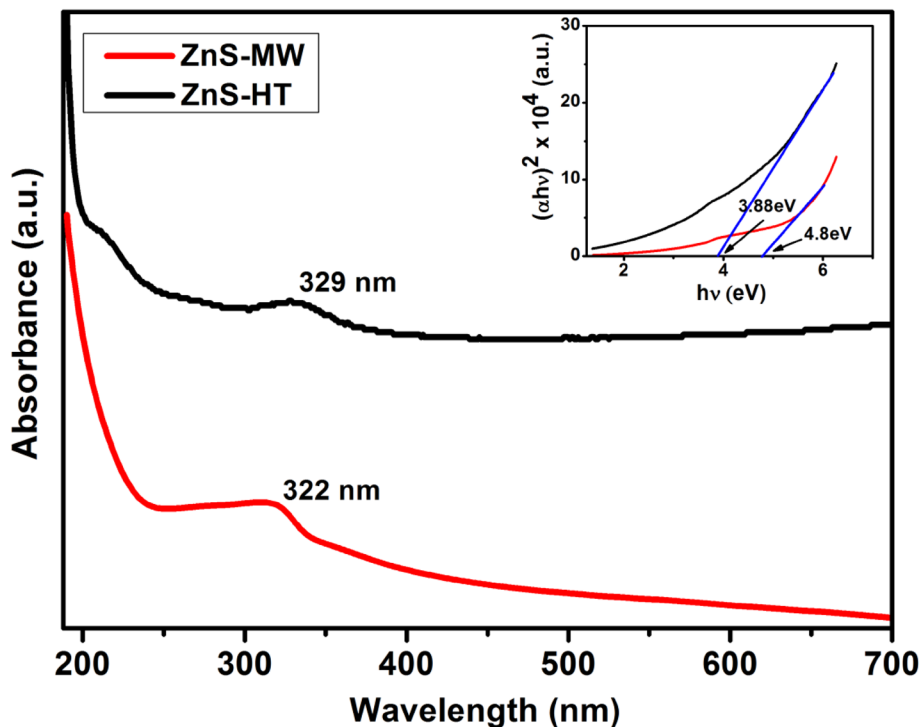
$t$  is the path length of radiation in sample solution.

Since ZnS is a direct band gap semiconductor, the exponent value of  $n = 1/2$  is considered for allowed direct transitions. From Eq. (3), the band gap  $E_g$  for nanoparticles was estimated by extrapolating the straight line portion of  $(\alpha h\nu)^2$  versus  $(h\nu)$  plot to the  $x$ -axis (Fig. 3). The obtained energy band gap of ZnS NPs was found to be 3.88 eV for ZnS-HT and 4.8 eV for ZnS-MW synthesized samples. This indicates a predominant blue shift in the energy band gap for the ZnS-MW samples. To explain such a blue shift, we have made use of the effective mass approximation model [23] according to which, the energy band gap of NP can be written as:

$$E_{np} = (E_g)_{bulk} + \frac{\hbar^2 \pi^2}{2R^2} \left( \frac{1}{m_e^*} + \frac{1}{m_h^*} \right) - \frac{1.8e^2}{4\pi\epsilon_0\epsilon_r R} \tag{5}$$

where  $R$  is the radius of nanoparticle.  $m_e^*$  is the effective mass of electron in ZnS =  $0.34 m_0$ ,  $m_h^*$  is the effective mass of hole =  $0.23 m_0$ ;  $m_0$  being rest mass of electron.  $\epsilon_r$ ,

Fig. 3 UV-Vis absorption spectra for ZnS-HT and ZnS-MW samples and inset is  $(\alpha h\nu)^2$  vs  $h\nu$  graph



is the dielectric constant of ZnS = 8.76;  $\epsilon_0$  is the permittivity of free space. Size of NPs, determined by the above relation is tabulated in Table 1. The slightly higher particle size obtained in UV–Vis studies compared to that of the structural studies for ZnS–MW sample could be due to the presence of energy states in the band gap which leads to an apparent change of band gap energy. Similar observation in the case CdS nanostructures was attributed to the effect of strains present in the sample [24]. Such strains were also present in our ZnS nanoparticles grown by both methods as it is evident from the XRD results presented in Table 1.

### 3.3.2 Photoluminescence (PL)

Photons of energy corresponding to the bandgap are used to excite the electrons from the valance band to conduction band (CB). The PL spectra for ZnS are observed in the visible region which may be due to point defects present in the crystal. Due to the high surface to volume ratio of nanoparticles at smaller dimensions, the defect density increases. The usual Schottky defects commonly present in ZnS are interstitial Zn ( $I_{Zn}$ ), interstitial S ( $I_S$ ), Zn vacancy ( $V_{Zn}$ ) and S vacancy ( $V_S$ ) [25].

Photoluminescence spectra of ZnS–HT and ZnS–MW samples are shown in Fig. 4a, b respectively. Broad and asymmetric spectra are observed for both type of samples, indicating the presence of more than one contributors to the PL intensity. Gaussian curve fitting was applied to deconvolute the PL curves. The best Gaussian fit gave five different peaks for both ZnS–HT and ZnS–MW. PL intensity for the ZnS–HT sample is higher due to better crystallinity possessed by it compared to ZnS–MW sample. The emission wavelengths near 360 nm in the samples have arisen due to transitions from interstitial Zn. The presence of excess Zn in the material gives rise to emission near 390 nm and it is attributed to changing Zn:S ratio [23]. In our studies, EDS spectra showed slight excess amount of Zn than the stoichiometric ratio of Zn:S = 1. The emissions at 350 nm and 442 nm in ZnS–MW are attributed to S interstitials and transition from surface sulfur vacancy to surface Zn vacancy respectively. The green PL peak at 511 nm is assigned to elemental sulfur species on the surface of ZnS [26].

Emission at 442 nm was not observed in ZnS–HT. This may be due to the filling up of surface sulfur vacancies by  $S^{2-}$  ions because of higher amount of sulfur present in ZnS–HT samples [27]. Conventional heating method has a larger capacity to eliminate the shallow defects while the microwave heating is unable to eliminate them [28]. Emission corresponding to 469 nm is related to recombination of electrons at S vacancy donor level with holes trapped at Zn vacancy acceptor level [29]. According to Sookhikian et al. [29] surface vacancy related states are shallow defect states; the energy difference between surface  $S^{2-}$  vacancies and

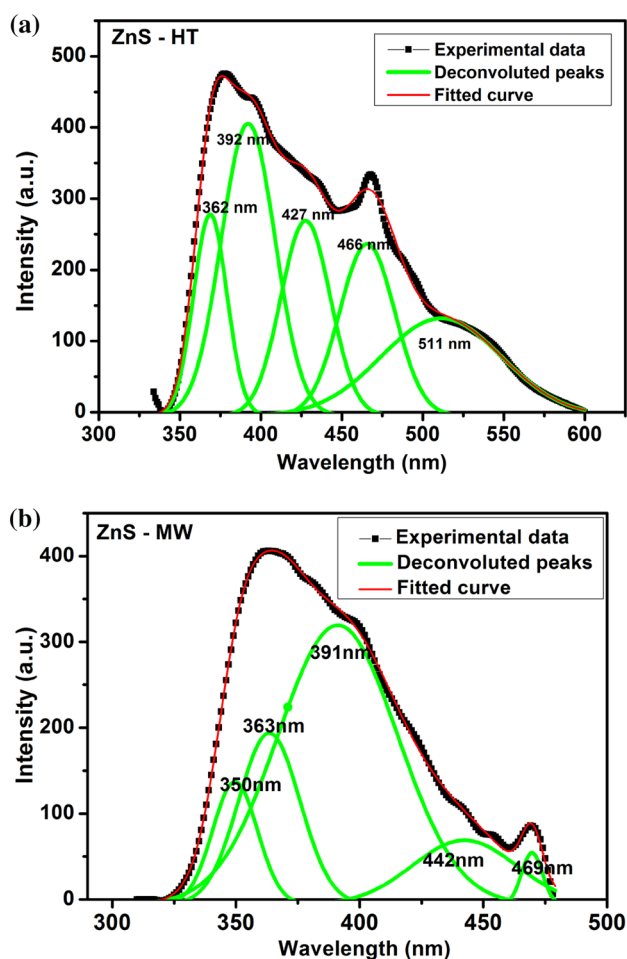


**Fig. 4** **a** Photoluminescence spectra for ZnS–HT sample. **b** Photoluminescence spectra for ZnS–MW samples

surface  $Zn^{2+}$  vacancies is slightly larger than that between internal  $S^{2-}$  vacancies ( $V_s$ ) and internal  $Zn^{2+}$  vacancies ( $V_{Zn}$ ).

Some of the PL peaks appear at nearly same wavelength positions in both the samples, but have different intensities. These are—peaks near 362 nm, 391 nm and 466 nm. Marginal shift in the emission peaks could be associated with the change in the particle size obtained by two methods. It appears that certain peaks are signature peaks and are intrinsic to the material depending on the precursor chosen and their ratio selected for synthesis procedure [30, 31]. The PL emission near 469 nm is very feeble for the ZnS–MW samples. The energy states within the band gap in the nanocrystals are produced due to surface states and/or  $Zn^{2+}$  or  $S^{2-}$  ions. The surface-related states result in emission due to recombination at 442 nm and the intrinsic Zn and S vacancies prevailed emissions at 469 nm. The peak around 442 nm is a broad and intense peak compared to emission at 469 nm indicating the presence of surface defect states dominated the PL emission spectra. The strongest emission

peak is due to excess zinc which is believed to be present at the surface of nanostructure. The transition taking place around 391 nm corresponds to transition from Zn interstitial to S interstitial states. So such transition occur at a lesser energy (3.17 eV) compared to the transitions around 362 nm (3.45 eV).

The reasons for the decrease in PL intensity in the case of ZnS–MW may be ascribed as follows: the nucleation and growth process of the ZnS crystallites are very quick, leading to the formation of defects. These defects on the surface of ZnS can trap the photo-induced electrons and holes. This will add to an increase in the charge separation on the ZnS nanospheres and decrease the recombination rate of the photo-induced electron and hole, resulting in a decrease in the PL intensity [32]. The presence of defects will strongly influence the dielectric and transport properties of the samples [33].

### 3.4 Dielectric studies

The technique of ac analysis has been widely used to investigate the dielectric behavior of amorphous and polycrystalline materials. The conductivity of semiconductor materials is known to be frequency dependent since it involves conduction between localized states [34]. Depending on the frequency of operation, a given dielectric material can possess one or more of these basic types of electric polarization: electronic, atomic (or ionic), dipolar (or rotational) and interface (or space charge) polarization. To understand the conduction mechanism involving defects state in the grown

nanoparticles, frequency dependent dielectric studies were carried out.

#### 3.4.1 Dielectric constant and dielectric loss

Figures 5 and 6 shows the variation of dielectric constant with frequency for the two samples ZnS–HT and ZnS–MW, respectively, at temperatures ranging from 223 to 323 K. The low-frequency dielectric constant ( $\epsilon'$ ) of both samples was observed to be higher than that of the bulk dielectric constant 9. This may be due to the increase in the interfacial polarization caused by larger grain boundary between the smaller grains and can be explained on the basis of Maxwell–Wagner model [35]. The model assumes a dielectric medium to be made up of conducting grains and relatively less conducting grain boundaries. The grain boundaries are more effective at low frequencies while the grains are highly active at high frequencies. A gradually decreasing trend of permittivity is observed with increasing frequency at all temperatures for both type of samples. At high frequencies, the dipoles can no longer follow the field and  $\epsilon'$  decreases.

The insets in Figs. 5 and 6 show the variation of dielectric loss ( $\epsilon''$ ) with frequency. The dielectric loss ( $\epsilon''$ ) decreases in the low-frequency region due to high resistivity of grain boundaries and energy expended for motion of charge carriers is high. With further increase in frequency,  $\epsilon''$  shows a maximum. This particular behavior suggests a dielectric relaxation process. The frequency corresponding to maximum  $\epsilon''$  is found to shift to higher frequencies with increasing temperature. This behavior is typical of polycrystalline

**Fig. 5** Variation of dielectric constant with frequency at different temperatures for ZnS–HT and inset is variation of dielectric loss with frequency

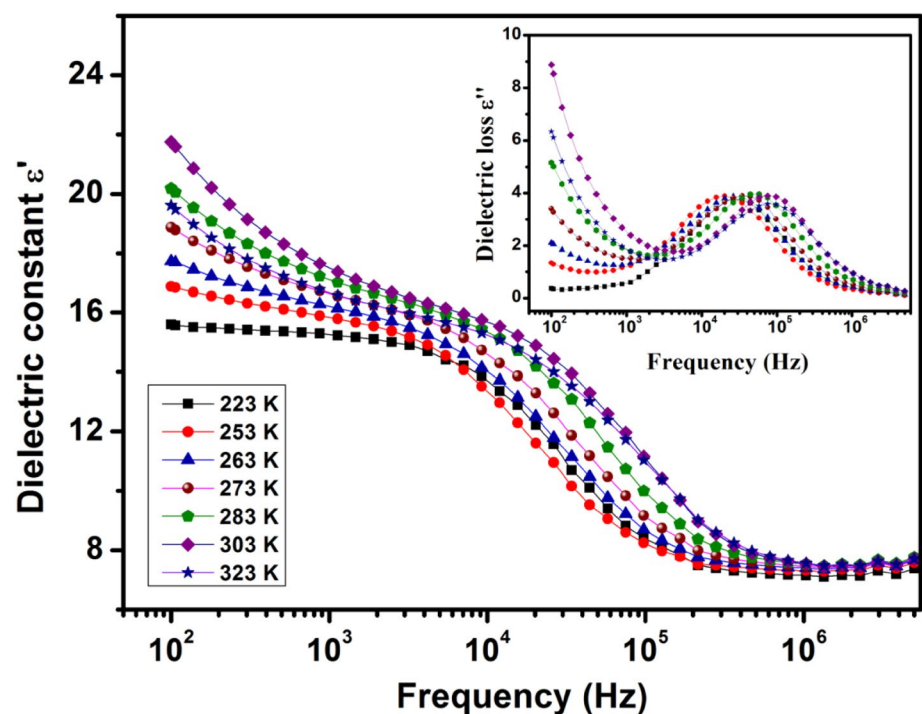
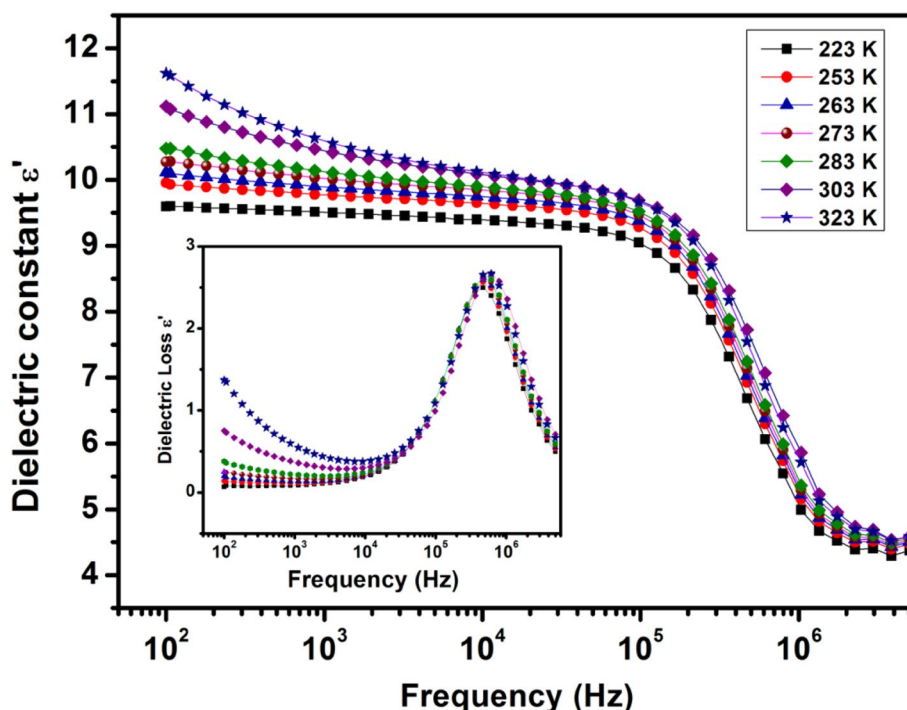


**Fig. 6** Variation of dielectric constant with frequency at different temperatures for sample ZnS–MW and inset is variation of dielectric loss with frequency



semiconducting material [36]. Thus the variation of peak frequency ( $f_{max}$ ) with temperature follows Arrhenius relation, supporting thermally activated process. We have plotted the Arrhenius plot of  $\log f_{max}$  versus  $1000/T$  for both samples. The activation energy  $E_a$  of relaxation process is calculated by plotting  $\log f$  versus  $1000/T$ , and using Arrhenius expression:

$$\text{Peak frequency } f = f_0 \exp\left(\frac{-E_a}{kT}\right), \tag{6}$$

$f_0$  is a constant,  $k$  Boltzmann constant.

In ZnS–MW sample, the relaxation peaks for various temperatures lie close to one another exhibiting very small activation energy. However, for ZnS–HT sample, the activation energy for this relaxation process is 0.184 eV.

### 3.4.2 AC conductivity

Measurement of the ac conductivity of semiconductors is a powerful tool for obtaining information about the defect states present in the system and the measurement helps to distinguish between localized and band to band (dc) conduction. Frequency dependence of conductivity for ZnS–HT and ZnS–MW samples at room temperature is shown in Figs. 7a and 8a, respectively. It can be seen that  $\sigma_{ac}$  does not change much but increases slightly with temperature in low frequency region. This may be attributed to the interfacial polarization caused due to grain boundaries which are highly resistive. Within the measured high-frequency limits, microwave

synthesized ZnS NPs show a higher conductivity by one order of magnitude compared to that of ZnS–HT. The low conductivity in ZnS–HT NPs may be due to the agglomeration of ZnS nanoparticles which offers high resistance due to enhanced inter-granular distance between the grains [37]. The conductivity increases with increase in temperature implies that ac conductivity is a thermally activated process.

Inset in Fig. 7a shows the conductivity as a function of frequency in double log representation. At higher frequencies, near the top of each of these curves there is contribution from grains which follow the universal dielectric response [38]. The dispersion region of  $\sigma_{ac}(\omega)$  is fitted with Jonscher’s power law by means of nonlinear least square fitting. Figure 7c represents the conductivity spectrum for ZnS–HT to which Jonscher’s model is fitted at high-frequency region. In Fig. 8b plot of  $\log \sigma_{ac}$  vs  $1000/T$  is shown.

The temperature dependences of ac conductivity of ZnS–MW samples are shown in Fig. 8a. Jonscher’s power law is fitted to conductivity spectrum for ZnS–MW sample at high-frequency region, as done in the case of ZnS–HT sample. Figure 8b shows a plot of  $\log \sigma_{ac}$  vs  $1000/T$ .

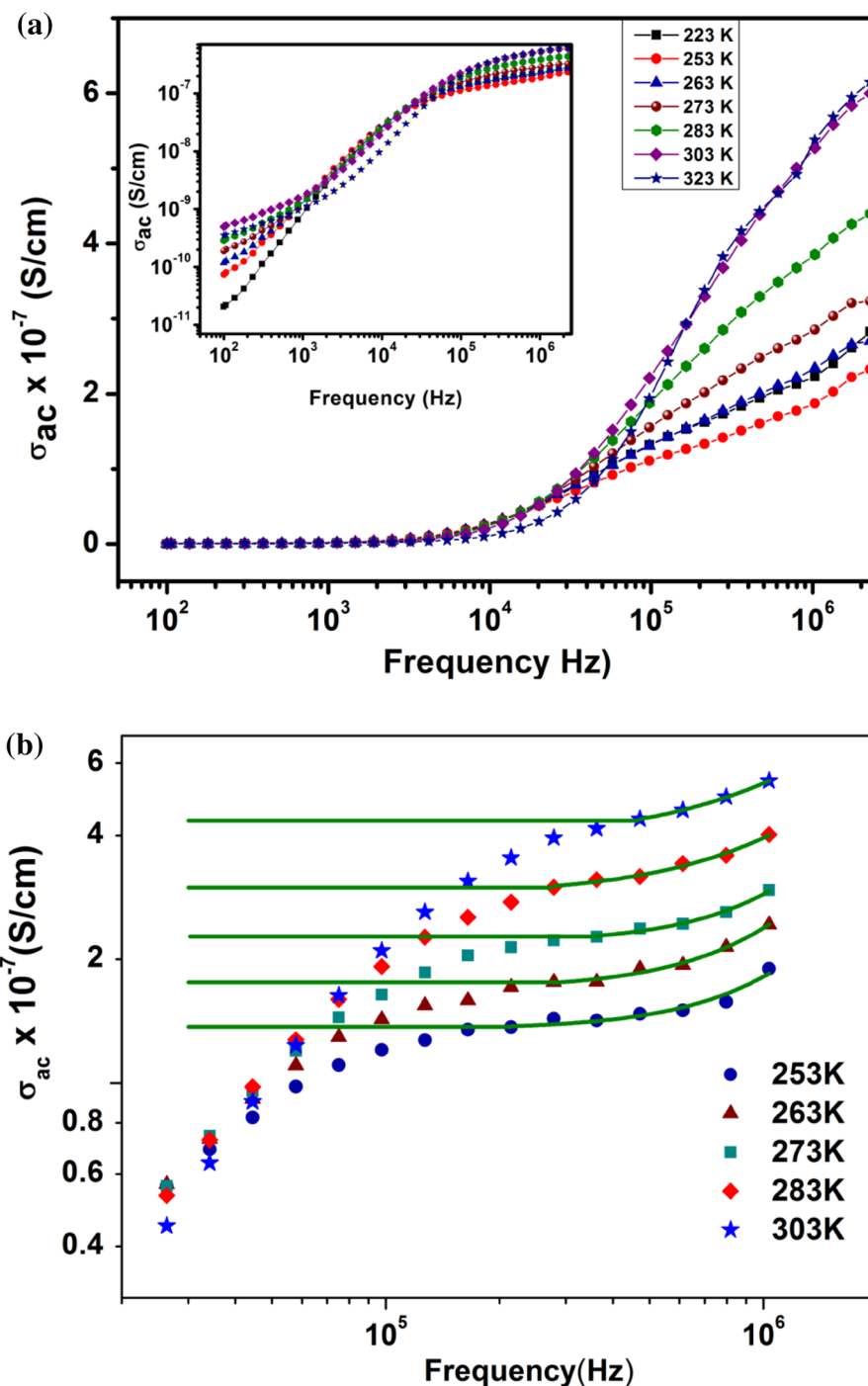
The dc conductivity,  $\sigma_{dc}$  values obtained are plotted against  $1000/T$ , slope of which is used to calculate activation energy  $E_a$  using the Arrhenius type of equation:

$$\sigma_{dc} = \sigma_0 \exp\left(-\frac{E_a}{KT}\right) \tag{7}$$

where  $\sigma_0$  is pre exponential factor. From the slopes of lines in Fig. 8b activation energy is calculated.  $E_a = 0.155$  eV for



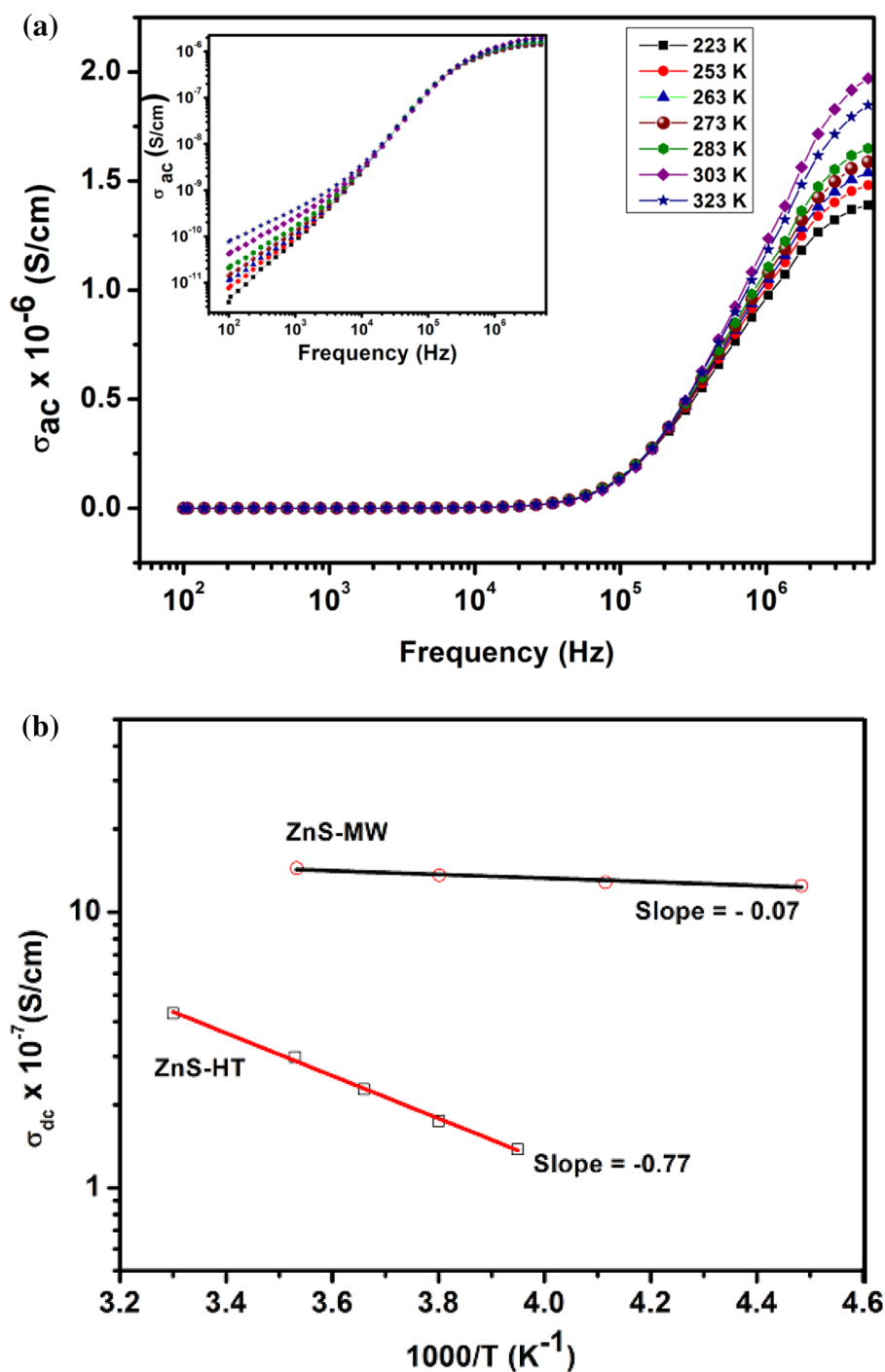
**Fig. 7** **a** Variation of  $\sigma_{ac}$  with frequency for ZnS-HT and inset is log-log plot of  $\sigma_{ac}$  and frequency. **b** log-log plot of  $\sigma_{ac}$  and frequency of ZnS-HT at select temperatures for the high-frequency region



ZnS-HT and  $E_a = 0.014$  eV for ZnS-MW sample. These values are nearly equal to  $E_a$  obtained in the case of dipolar relaxation as explained in the previous section. Moreover, these values are much smaller than the band gap value (3.68 eV). A possible reason for small values of  $E_a$  is due to the presence of various defects present in the band gap as evidenced by photoluminescence spectra. Since ZnS-MW contains more number of defects compared to ZnS-HT, activation energy is very small. Hence dc conductivity might

have arisen by the excitation of electrons from localized states to the conduction band. It has been reported that the low value of activation energy have arisen due to dipolar relaxations between polaronic type defects present within the band gap [36, 39]. Further, the ZnS-HT sample exhibited a near stoichiometry compared to the ZnS-MW, a low density of charged defects may be present in the former case.

**Fig. 8** **a** Variation of  $\sigma_{ac}$  with frequency for ZnS–MW and inset is log–log plot of  $\sigma_{ac}$  and frequency. **b** Plot of  $\log \sigma_{ac}$  vs  $1000/T$  for ZnS–HT and ZnS–MW samples



## 4 Conclusion

In summary, structural, optical and electrical properties of the synthesized ZnS NPs by microwave heating and conventional heating methods were compared. Formation of nanocrystalline phase with a preferred (111) orientation for the samples grown by both methods was confirmed by X-ray diffraction studies. Crystallite size was found to depend on the method of preparation of the NPs and microwave heating

method seems to be beneficial for obtaining fine grain structures. UV–Vis absorption spectra exhibited a blue shift in absorption peak for the ZnS–MW and the quantum confinement effect resulted in an increased band gap energy compared to that of ZnS–HT. Size of NPs determined by XRD, UV–absorption spectra and TEM complement each other. The higher PL intensity observed in ZnS–HT could be attributed to the better crystallinity. On the other hand, the strained ZnS–MW samples exhibited PL peaks due

to surface related defects. The electrical studies have also confirmed the presence of larger number of defects. Lower activation energy for dipolar relaxation and dc conductivity was observed for ZnS–MW samples. Microwave synthesized samples when stabilized may find application in degradation of pollutant molecules, without producing secondary by-products and also due to low activation energy such materials are suitable for various switching applications.

**Acknowledgements** The authors thank UGC-DAE Consortium for Scientific Research, Mumbai Centre for dielectric measurements, DST-SAIF centre at Karnatak University-Dharwad for photoluminescence measurements, Manipal Academy of Higher Education- Manipal for other characterisations and Bhandarkars' Arts and Science college, Kundapura for sample preparation facilities. One of the authors, Lalitha Devi B thanks the University Grants Commission, Government of India, for teacher fellowship.

### Compliance with ethical standards

**Conflict of interest** The authors declare that they have no conflict of interest.

### References

1. A.P. Alivisatos, Semiconductor clusters, nanocrystals, and quantum dots. *Science* **271**, 933 (1996)
2. X. Fang, T. Zhai, U.K. Gautam, L. Li, L. Wu, Y. Bando, D. Golberg, ZnS nanostructures: from synthesis to applications. *Prog. Mater. Sci.* **56**, 175 (2011)
3. D.W. Synnott, M.K. Seery, S.J. Hinder, G. Michlits, S.C. Pillai, Anti-bacterial activity of indoor-light activated photocatalysts. *Appl. Catal. B Environ.* **130–131**, 106 (2013)
4. J. Souriau, Y. Dong, J. Penczek, H.G. Paris, C.J. Summers, Cathodoluminescent properties of coated SrGa<sub>2</sub>S<sub>4</sub>: Eu<sup>2+</sup> and ZnS:Ag, Cl phosphors for field emission display applications. *Mater. Sci. Eng. B* **76**, 165 (2000)
5. I.O. Oladeji, L. Chow, Synthesis and processing of CdS/ZnS multilayer films for solar cell application. *Thin Solid Films* **474**, 77 (2005)
6. M. Koneswaran, R. Narayanaswamy, L-Cysteine-capped ZnS quantum dots based fluorescence sensor for Cu<sup>2+</sup> ion. *Sensors Actuators, B Chem.* **139**, 104 (2009)
7. Z. Li, J. Wang, X. Xu, X. Ye, The evolution of optical properties during hydrothermal coarsening of ZnS nanoparticles. *Mater. Lett.* **62**, 3862 (2008)
8. C. Ramamoorthy, V. Rajendran, Formation of solid and hollow sphere ZnS nanoparticles by hydrothermal process and their structural, optical and photocatalytic activity. *Appl. Phys. A* **124**, 500 (2018)
9. N.I. Kovtyukhova, E.V. Buzaneva, C.C. Waraksa, T.E. Mallouk, Ultrathin nanoparticle ZnS and ZnS: Mn films : surface sol–gel synthesis, morphology, photophysical properties. *Mater. Sci. Eng. B* **70**, 411 (2000)
10. J. Yuan, K. Kajiyoshi, K. Yanagisawa, Fabrication of silica nano-coatings on ZnS–type phosphors via a sol–gel route using cetyltrimethylammonium chloride dispersant. *Mater. Lett.* **60**, 1284 (2006)
11. J.F. Xu, W. Ji, J.Y. Lin, S.H. Tang, Y.W. Du, Preparation of ZnS nanoparticles by ultrasonic radiation method. *Appl. Phys. A* **641**, 639 (1998)
12. R.S. Sudar, D. Pukazhselvan, C.K. Mahadevan, Studies on the synthesis of cubic ZnS quantum dots, capping and optical–electrical characteristics. *J. Alloys Compd.* **517**, 139 (2012)
13. U. Baishya, D. Sarkar, ZnS nanocomposite formation: effect of ZnS source concentration ratio. *Indian J. Pure Appl. Phys.* **49**, 186 (2011)
14. K.J. Rao, B. Vaidyanathan, M. Ganguli, P.A. Ramakrishnan, Synthesis of inorganic solids using microwaves. *Chem. Mater.* **11**, 882 (1999)
15. S. Naweem Dahal, J. Garcia, S.M. Zhou, Humphrey, Beneficial effects of microwave-assisted heating versus conventional heating in noble metal nanoparticle synthesis. *ACS Nano* **6**, 9433 (2012)
16. J. Zhu, M. Zhou, J. Xu, X. Liao, Preparation of CdS and ZnS nanoparticles using microwave irradiation. *Mater. Lett.* **47**, 25 (2001)
17. Y. Zhao, J.M. Hong, J.J. Zhu, Microwave-assisted self-assembled ZnS nanoballs. *J. Cryst. Growth* **270**, 438 (2004)
18. Q. Ma, Y. Wang, J. Kong, H. Jia, Tunable synthesis, characterization and photocatalytic properties of various ZnS nanostructures. *Ceram. Int.* **42**, 2854 (2016)
19. B.D. Cullity, Elements of X-ray diffraction, 2nd edn. (Addison Wiley Publishing Company, Newyork, 1972), p. 110
20. S. Lee, D. Song, D. Kim, J. Lee, S. Kim, I.Y. Park, Y.D. Choi, Effects of synthesis temperature on particle size/shape and photoluminescence characteristics of ZnS:Cu nanocrystals. *Mater. Lett.* **58**, 342 (2004)
21. A.L. Rogach, A. Kornowski, M. Gao, A. Eychmüller, H. Weller, Synthesis and characterization of a size series of extremely small thiol-stabilized CdSe nanocrystals. *J Phys Chem B* **103**, 3065 (1999)
22. J. Tauc, Menth, states in Gap. *J Non-crystalline Solids* **8**, 569 (1972)
23. L. E. Brus, electron–electron and electron-hole interactions in small semiconductor crystallites: the size dependence of the lowest excited electronic state. *J Chem. Phys* **80**, 4403 (1984)
24. S. Mondal, S. Sudhu, S. Bhattacharya, S.K. Saha, Strain-induced tunable band gap and morphology-dependent photocurrent in RGO–CdS nanostructures. *J. Phys. Chem. C* **119**, 27749 (2015)
25. D. Denzler, M. Olschewski, K. Sattler, Luminescence studies of localized gap states in colloidal ZnS nanocrystals. *J. Appl. Phys.* **84**, 2841 (1998)
26. A.K. Kole, P. Kumbhakar, Effect of manganese doping on the photoluminescence characteristics of chemically synthesized zinc sulfide nanoparticles. *Appl. nano sci* **2**, 15 (2012)
27. J.F. Suyver, S.F. Wuister, J.J. Kelly, A. Meijerink, Synthesis and photoluminescence of nanocrystalline ZnS: Mn<sup>2+</sup>. *Nano Lett.* **1**, 429 (2001)
28. J. Bohnemann, R. Libanori, M.L. Moreira, E. Longo, High-efficient microwave synthesis and characterisation of SrSnO<sub>3</sub>. *Chem. Eng. J.* **155**, 905 (2009)
29. M. Sookhakian, Y.M. Amin, W.J. Basirun, M.T. Tajabadi, N.Kamarulzaman Synthesis, structural and optical properties of type-II ZnO–ZnS core–shell nanostructure. *J. Lumin.* **145**, 244 (2014)
30. B. Poornaprakash, U. Chalapathi, S.V.P. Vattikuti, Optical, and magnetic properties of Fe, Co, and Ni doped ZnS nanoparticles. *Appl. Phys. A* **123**, 275 (2017)
31. N. Karar, Photoluminescence from doped ZnS nanostructures. *Solid State Commun.* **142**, 261 (2007)
32. X. Liu, Z. Li, C. Zhao, W. Zhao, J. Yang, Y. Wang, F. Li, Facile synthesis of core–shell CuO/Ag nanowires with enhanced photocatalytic and enhancement in photocurrent. *J. Colloid Interface Sci.* **419**, 9 (2014)
33. K.C. Anoop Chandran, George, Defect induced modifications in the optical, dielectric, and transport properties of hydrothermally

- prepared ZnS nanoparticles and nanorods. *J. Nanopart. Res.* **16**, 2238 (2014)
34. R. Gerhardt, Impedance and dielectric spectroscopy revisited—distinguishing localised relaxations from long range conductivity. *J. Phys.Chem.Solids* **55**, 1491 (1994)
  35. J.C. Maxwell, *A Treatise on Electricity and Magnetism* (Oxford University Press, New York, 1973)
  36. T. Shekharam, V.L. Rao, G. Yellaiah, T.M. Kumar, M. Nagabhushanam, AC conductivity, dielectric and impedance studies of  $\text{Cd}_{0.8x}\text{Pb}_x\text{Zn}_{0.2}\text{S}$  mixed semiconductor compounds. *J. Alloys Compd.* **617**, 952 (2014)
  37. A.S. Roy, S. Gupta, S. Sindhu, A. Parveen, P.C. Ramamurthy, Dielectric properties of novel PVA/ZnO hybrid nanocomposite films. *Compos. Part B Eng.* **47**, 314 (2013)
  38. A.K. Jonscher, A new understanding of the dielectric relaxation of solids. *J. Mater. Sci.* **16**, 2037 (1981)
  39. A. Artemenko, S. Payan, A. Rousseau, D. Levasseur, E. Arveux, G. Guegan, M. Maglione, Low temperature dielectric relaxation and charged defects in ferroelectric thin films Low temperature dielectric relaxation and charged defects in ferroelectric thin films. *AIP Adv.* **3**, 0 42111 (2013)